CHEMISTRY

Formation of the elusive tetrahedral P_3N molecule

Chaojiang Zhang[1,2], Cheng Zhu[1,2], André K. Eckhardt[3]*, Ralf I. Kaiser[1,2]*

The tetrahedral 1,2,3-triphospha-4-azatricyclo [1.1.0.0^{2,4}] butane (P_3N) molecule—an isovalent species of phosphorus (P_4)—was prepared in low-temperature (5 K) phosphine-nitrogen ices and was identified in the gas phase through isomer-selective, tunable, soft photoionization reflectron time-of-flight mass spectrometry. Theoretical calculations reveal that the substitution of a single phosphorus atom by nitrogen in the P_4 molecule results in enhanced spherical aromaticity while simultaneously increasing the strain energy from 74 to 195 kJ mol^{-1}. In P_3N, the P—P bond is shortened compared to those in P_4 by 3.6 pm, while the P—N—P bond angle of 73.0° is larger by 13.0° compared to the P—P—P bond angle of 60.0° in P_4. The identification of tetrahedral P_3N enhances our fundamental understanding of the chemical bonding, electronic structure, and stability of binary, interpnictide tetrahedral molecules and reveals a universal route to prepare ring strained cage molecules in extreme environments.

INTRODUCTION

Since the discovery of white phosphorus (P_4, **2**) by Hennig Brand 350 years ago (*1*, *2*), tetrahedral molecules composed of pnictide atoms (group XV; Fig. 1) such as tetranitrogen (N_4, **1**) (*3*), tetraarsenic (As_4, **3**) (*4*, *5*), and tetrantimony (Sb_4, **4**) (*6*) have intrigued the inorganic preparative (*7*, *8*), theoretical (*9*, *10*), and physical chemistry communities (*11*, *12*) from the fundamental viewpoints of electronic structure theory and chemical bonding along with their potential as high energy density materials (*13*). These tetrahedral (T_d) molecules represent the simplest prototypes of spherical aromaticity structures—a concept originally developed by Hirsch *et al.* to determine to what extent fullerenes and polyhedral boranes are aromatic and then expanded to tetrahedral cage molecules (*14*, *15*). Considering the ring strain energies of, e.g., 225.6 and 74.1 kJ mol^{-1} for **1** and **2**, respectively, along with their inherent high reactivity and difficulties of a directed synthesis of pnictide tetrahedral molecules (*16*), increasing computational and preparative attention has been devoted to isolate binary, interpnictide tetrahedral molecules (*17*, *18*). Early gas-phase Raman spectroscopy of mixed phosphorus and arsenic vapors at 1273 K by Ozin (*19*) provided compelling evidence on the existence of three binary pnictogen tetrahedral molecules (AsP_3, **5**; As_2P_2, **6**; As_3P, **7**); the concept of preparing mixed pnictogen tetrahedral species under thermal equilibrium conditions was also expanded to incorporate the isovalent antimony element (SbP_3, **8**) (*19*). Cummins *et al.* developed a formidable preparative synthetic approach to binary pnictogen tetrahedral molecules exploiting transition metal complexes acting as effective anionic cyclic triphosphorus (P_3^{3-}) transfer agents; when combined with an electrophile (E^{3+}; E = P, As, Sb), P_4 (**2**), AsP_3 (**5**), and SbP_3 (**8**) were prepared (*20*–*25*). This strategy was expanded to synthesize the tetrahedron 1,2,3-triphospha tricyclo [1.1.0.0^{2,4}] butane (P_3CH, **9**) (*26*).

Despite this remarkable progress on the synthesis of interpnictide tetrahedral molecules, the preparation of the C_{3v} symmetric, tetrahedral molecule 1,2,3-triphospha-4-azatricyclo [1.1.0.0^{2,4}] butane (P_3N, **10**; Fig. 1) represents a fundamental synthetic challenge contemplating a notable ring strain energy of 195.1 kJ mol^{-1} calculated at the CBS-QB3//B3LYP/cc–pVTZ level of theory and, hence, tendency to ring-open or polymerize. Electronic structure calculations challenge the proposed instability and predicted that P_3N (**10**) represents a global minimum and, hence, is both thermodynamically and kinetically stable toward unimolecular decomposition once prepared (*27*). However, a traditional high-temperature gas phase synthesis from white phosphorus (P_4) and nitrogen (N_2) is problematic; the cleavage of the nitrogen-nitrogen triple bond, which has a bond energy of 945 kJ mol^{-1}, in a fraction of only 10^{-4} of the nitrogen molecules would require at least 10,000 K—a temperature much higher than the surface of our Sun (5778 K). Along with the lack of a classical synthetic chemistry route using anionic cyclic triphosphorus (P_3^{3-}) transfer agents in conjunction with an N^{3+} electrophile in solution, a strategy exploiting nonequilibrium chemistry is required for the preparation of the hitherto elusive P_3N (**10**) molecule in extreme environments. Consequently, binary pnictogen tetrahedral molecules carrying nitrogen and phosphorus represent one of the least explored classes of inorganic molecules.

Here, we reveal the first preparation of the C_{3v} symmetric, P_3N (**10**) molecule, 1,2,3-triphospha-4-azatricyclo [1.1.0.0^{2,4}] butane, the isovalent counterpart of the P_4 (**2**) molecule, through exposure of low-temperature (5 K) phosphine (PH_3)–nitrogen (N_2) ices to energetic electrons via transient reactants carrying the neutral cyclic triphosphorus moiety (*c*-P_3). Combined with electronic structure calculations, tetrahedral P_3N (**10**) is explicitly identified upon the temperature-programmed desorption (TPD) phase of the irradiated ices via isomer-selective photoionization in the gas phase based on computed adiabatic ionization energies (IEs) of distinct P_3N isomers (Fig. 2 and table S1) exploiting vacuum ultraviolet (VUV) photoionization reflectron time-of-flight mass spectrometry (PI-ReTOF-MS). Electronic structure calculations reveal that P_3N (**10**) can be formed via decomposition of three cyclic H_2NP_3 (*c*-H_2NP_3) transients (**13** to **15**) through the concerted molecular hydrogen loss. The first preparation and identification of P_3N (**10**) showcases its gas phase stability over at least 10 μs as demonstrated in the present study. These findings not only advance our fundamental knowledge on the chemical bonding and electronic structure of strained, interpnictide tetrahedral molecules but also provide a powerful strategy to prepare highly strained, still elusive interpnictides such as PN_3 and P_2N_2 through nonequilibrium chemistry in exotic low-temperature environments, which traditionally "should not exist."

[1]Department of Chemistry, University of Hawaii at Manoa, 2545 McCarthy Mall, Honolulu, HI 96822, USA. [2]W. M. Keck Laboratory in Astrochemistry, University of Hawaii at Manoa, 2545 McCarthy Mall, Honolulu, HI 96822, USA. [3]Lehrstuhl für Organische Chemie II, Ruhr-Universität Bochum, 44801 Bochum, Germany.
*Corresponding author. Email: andre.eckhardt@rub.de (A.K.E.); ralfk@hawaii.edu (R.I.K.)

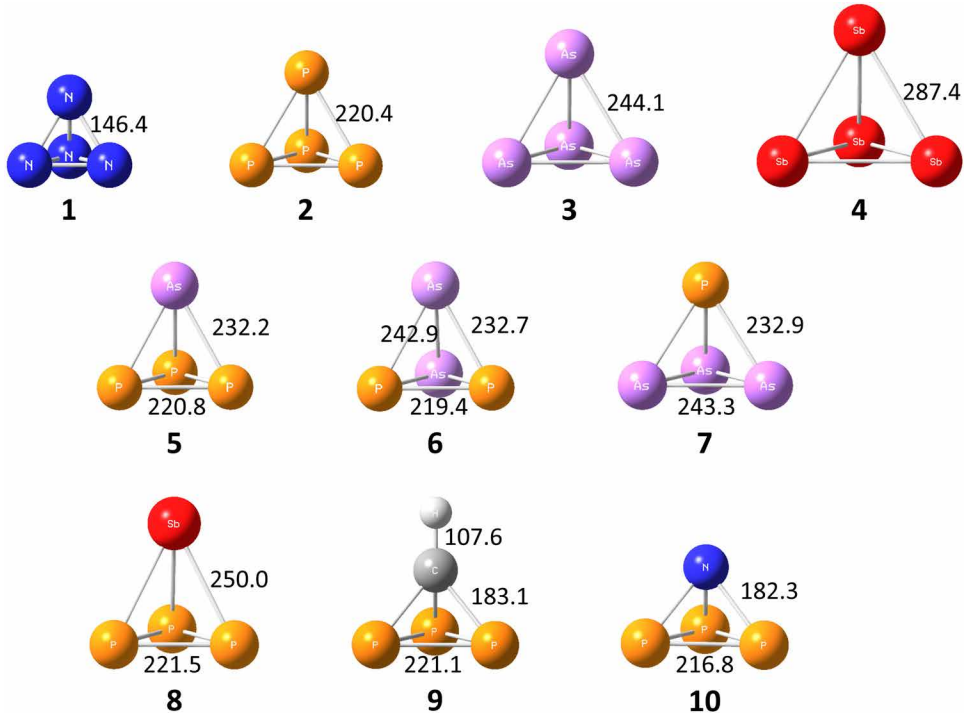

Fig. 1. Structures of tetrahedrally shaped molecules carrying group XV atoms. Tetraazatetrahedrane (N_4, **1**) has only been subject to computational studies; tetraphosphorus (P_4, **2**), tetraarsenic (As_4, **3**), tetraantimony (Sb_4, **4**), 1,2,3-triphospha-4-arsatricyclo [1.1.0.0^{2,4}] butane (P_3As, **5**), 1,2-diphospha-3,4-diarsatricyclo [1.1.0.0^{2,4}] butane (P_2As_2, **6**), 1-phospha-2,3,4-triarsatricyclo [1.1.0.0^{2,4}] butane (PAs_3, **7**), and 1,2,3-triphospha-4-stibatricyclo [1.1.0.0^{2,4}] butane (P_3Sb, **8**) have been isolated. Bond lengths are given in picometers (pm) with atoms color coded in blue (nitrogen), orange (phosphorus), purple (arsenic), red (antimony), gray (carbon), and white (hydrogen). Structures of the isoelectronic 1,2,3-triphosphatricyclo [1.1.0.0^{2,4}] butane (P_3CH, **9**) and 1,2,3-triphospha-4-azatricyclo [1.1.0.0^{2,4}] butane (P_3N, **10**) molecules are also shown.

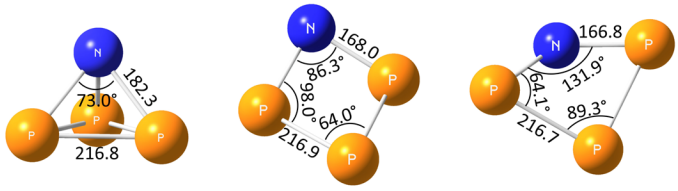

10, C_{3v}, $^1A_1$
9.33–9.48 eV
0.0 kJ mol^{-1}

11, C_s, $^1A'$
8.31–8.46 eV
+114.8 kJ mol^{-1}

12, C_s, $^1A'$
7.83–7.98 eV
+186.1 kJ mol^{-1}

Fig. 2. Molecular structure of distinct P_3N isomers. Bond lengths are given in picometers (pm) and bond angles in degrees; point groups, electronic ground states, computed adiabatic IEs corrected for the electric field effect (blue), and relative energies (red) are also shown. The energies were computed at the CCSD(T)/CBS//B3LYP/cc–pVTZ + zero-point vibrational energy (ZPVE) level of theory. The atoms are color coded in blue (nitrogen) and orange (phosphorus).

RESULTS

After the exposure of the PH_3-N_2 ices to energetic electrons at 5 K, the irradiated ices were sublimed at a rate of 1 K min^{-1} to 300 K while probing the subliming molecules in the gas phase via PI-ReTOF-MS (*28*). This methodology denotes an extraordinary technique of detecting gas phase molecules isomer-selectively exploiting soft photoionization on the basis of their distinct adiabatic IEs through methodically tuning the photon energies (PEs) above and below the IE of the isomer of interest. This certifies the identity of the parent ions at a well-defined mass to charge ratio (m/z). The isomer-selective photoionization and, hence, identification of P_3N (**10**) requires the computation of the IEs of distinct P_3N isomers (Fig. 2). At the CCSD(T)/CBS//B3LYP/cc–pVTZ plus zero-point vibrational energy (ZPVE) level of theory, the calculations reveal the existence of three structural isomers **10**, **11**, and **12**. The C_{3v} symmetric tetrahedral isomer P_3N (**10**) represents the global minimum and is thermodynamically preferred compared to the nonplanar, C_s symmetric structures **11** and **12** by 114.8 and 186.1 kJ mol^{-1}, respectively. The IEs of these isomers were computed to be 9.33 to 9.48 (**10**), 8.31 to 8.46 (**11**), and 7.83 to 7.98 eV (**12**), accounting for the computational accuracies and the shift of up to 0.03 eV by the electric field of the ion optics (table S1). Accounting for the computed IEs of isomers **10** to **12**, two distinct PEs of 10.49 and 8.53 eV had to be selected to manifest the identity of P_3N (**10**). Photons at 10.49 eV can ionize all isomers. The recorded TPD profile at m/z = 107 (P_3N) reveals ion counts from 165 to 225 K with a distribution maximum close to 195 K (Fig. 3A). A separate experiment, which replaces nitrogen by 15-nitrogen ($^{15}N_2$), shifts this TPD profile from m/z = 107 to 108. This finding reveals that the carrier of the ions at m/z = 107 contains a single nitrogen atom [14 atomic mass unit (amu)] with the remaining mass accountable by three phosphorus atoms (93 amu). Therefore, the molecular formula of this species can only be assigned to P_3N. When the PE was tuned down to 8.53 eV, i.e., below the IE of **10** but above the IEs of **11** and **12**, the peak at m/z = 107 vanishes (Fig. 3B). These findings provide compelling evidence that the signal at m/z = 107 obtained with PE = 10.49 eV can only originate from isomer **10** but not from isomer **11** or **12**.

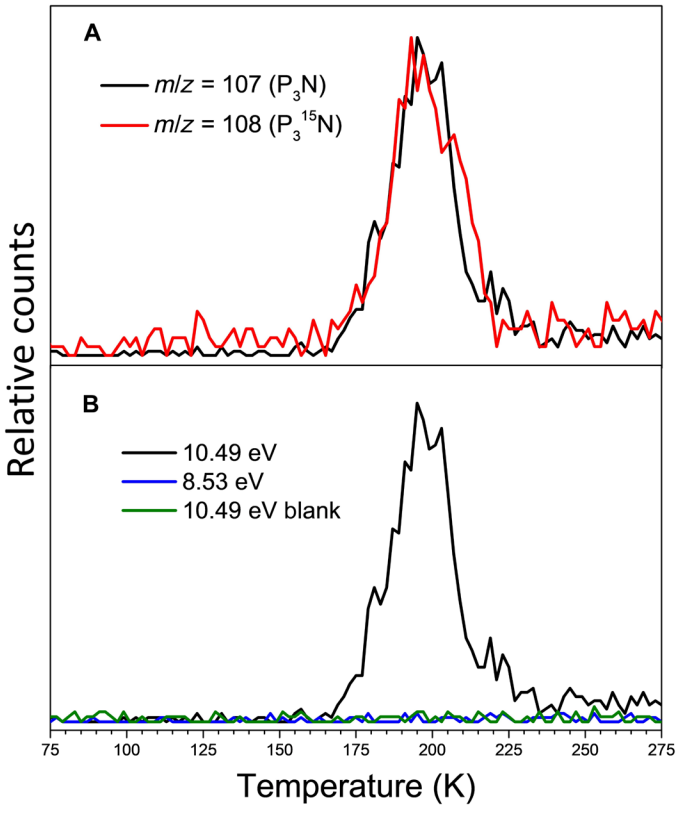

Fig. 3. PI-ReTOF-MS data were recorded during the temperature-TPD phase of processed phosphine (PH_3)–nitrogen (N_2) ices. (**A**) PI-ReTOF-MS signal recorded from the electron-processed PH_3-N_2 ice (black) and PH_3-$^{15}N_2$ ice (red) at a photon energy (PE) of 10.49 eV. (**B**) PI-ReTOF-MS signals at $m/z = 107$ detected during the TPD phase of the electron-processed PH_3-N_2 ices with PEs of 10.49 eV (black), 8.53 eV (blue), and 10.49 eV blank (green).

We also conducted the blank experiment by subliming nonirradiated PH_3-N_2 ices at PE = 10.49 eV. No sublimation event was detected at $m/z = 107$ (Fig. 3B), verifying that the P_3N (**10**) molecule requires radiolysis of PH_3-N_2 ices, but it is not the result of ion-molecule reactions in the gas phase upon sublimation of the reactants. Considering the average velocity of 174 m s^{-1} of P_3N (**10**) subliming at 195 K and the distance of 2 mm between the ice surface and the photoionization laser, the lifetimes of P_3N (**10**) in the gas phase exceed 11 ± 1 μs to survive the flight time from the sublimation to the photoionization region. Likewise, the lifetime of singly ionized P_3N (**10**) is at least 47 ± 1 μs to fly from the ionization region to the multichannel plate (MCP) of the detector, where $m/z = 107$ is eventually detected. Note that, traditionally, infrared spectroscopy has been used to assign unique vibration modes of newly formed molecules, too. In the present study, the exposure of the PH_3-N_2 ices to energetic electrons leads to two shoulders at 2270 and 1063 cm^{-1} along with a distinct absorption peak at 788 cm^{-1} (fig. S1 and table S2) (*29*). These features can be linked to stretching modes of P—H, PH_2 scissoring modes, and P—N ring deformation modes, respectively (*30*). The replacement of nitrogen by 15-nitrogen (^{15}N) that red-shifted the 788 cm^{-1} feature to 784 cm^{-1} suggests that this fundamental might be associated with a moiety-carrying nitrogen. With a scaling factor of 0.97 (*31*), the computed value of the P—N ring deformation mode (ν_6 = 809 cm^{-1}) for P_3N (**10**) (table S5) corresponds nicely to the experimentally observed 788 cm^{-1} feature. The remaining absorptions are beyond the cutoff of the infrared detector (fig. S1 and table S5). Consequently, in the present situation, infrared spectroscopy cannot be exploited to unambiguously assign P_3N (**10**), also because the electron exposure synthesizes a wide range of new molecules whose absorptions of the functional groups often overlap in the infrared regime.

Having identified the tetrahedral molecule 1,2,3-triphospha-4-azatricyclo [1.1.0.$0^{2,4}$] butane (P_3N, **10**) via PI-ReTOF-MS, we are shifting our attention now to its computed electronic and geometric structure. Compared to the tetrahedral P_4 (**2**), the replacement of a single phosphorus atom by isovalent atomic nitrogen reduced the symmetry of the P_3N (**10**) molecule to a C_{3v} point group and a $^1A_1$ electronic state (Fig. 2). The slightly distorted regular tetrahedron can be rationalized by inspecting the P—P and P—N bond lengths and bond angles. At the B3LYP/cc–pVTZ level of theory, the P—N bond and P—P bond lengths are computed to be 182.3 and 216.8 pm, with the latter shorter than the P—P bond of 220.4 pm in P_4 (**2**) (Fig. 1). This trend is also reflected in a lengthening of the bond from P—N via P—P, P—As, and P—Sb from 216.8, 220.4, 232.2, and 250.0 pm, as the atomic radii of the group XV element increases from nitrogen to antimony (*32*). In addition, the nitrogen substitution of P_4 (**2**) results in the bond angle of ∠P—N—P = 73.0° of P_3N (**10**), larger by 13.0° compared to the bond angle of ∠P—P—P = 60.0° in P_4 (**2**). An electronic property of note for comparison among N_4 (**1**), P_4 (**2**), and P_3N (**10**) is the degree of spherical aromaticity. Hirsch and co-workers have previously calculated large negative values for the nucleus-independent chemical shifts (NICSs) at the cage centers of T_d symmetrical clusters, including N_4 (**1**) and P_4 (**2**) (*14*, *15*). This was interpreted as spherical aromaticity and large diamagnetic ring currents in the tetrahedrons. Our calculated NICS value for P_3N (**10**) of −73.7 is more negative than for P_4 (**2**) of −61.3 and similar to N_4 (**1**) of −73.8. The calculated NICS value for the center of the cyclic P_3 moieties in P_4 (**2**) is −59.8 and only slightly lower than in the center of the three-dimensional tetrahedron. The NICS value for the center of the P_3 unit in P_3N (**10**) is −55.9 and −61.7 for the three P_2N units. Both values are much lower than the calculated value for the cage center; these results indicate that the NICS values correlate with the size of the elements in the cluster, which also affects the relative energy of the a_1 orbital (vide infra; Fig. 4 and table S8) (*14*). Despite the lowering in molecular symmetry upon going from T_d P_4 (**2**) to C_{3v} symmetric P_3N (**10**), spherical aromaticity is gained. This gain of spherical aromaticity is partially due to the fact that P_3N (**10**) similar to P_4 (**2**) maintains closed-shell σ and π subsystems (fig. S2), resulting in symmetrically distributed angular momenta. Electrons within the frontier orbital region are the most mobile and contribute predominantly to the ring-current effect. Therefore, the diatropic character of these clusters is mainly determined by the σ electrons (*14*). The increase in spherical aromaticity in P_3N (**10**) in comparison to P_4 (**2**) and P_3As (**5**) might be explained by the energetically higher lying a_1 (−7.62 eV) highest occupied molecular orbital (HOMO)–1 frontier orbital, which increases the electron density and ring current effect in P_3N (**10**) (Fig. 4, bottom) (*24*). The HOMO–LUMO (lowest unoccupied molecular orbital) energy gap in P_3N (**10**) (6.09 eV) is lower than in P_4 (**2**) (6.34 eV). We calculated the relative strain energies of N_4 (**1**), P_4 (**2**), and P_3N (**10**) using a series of homodesmotic equations as depicted in Fig. 4 (top). Despite the acute bond angles in P_4 (**2**), the

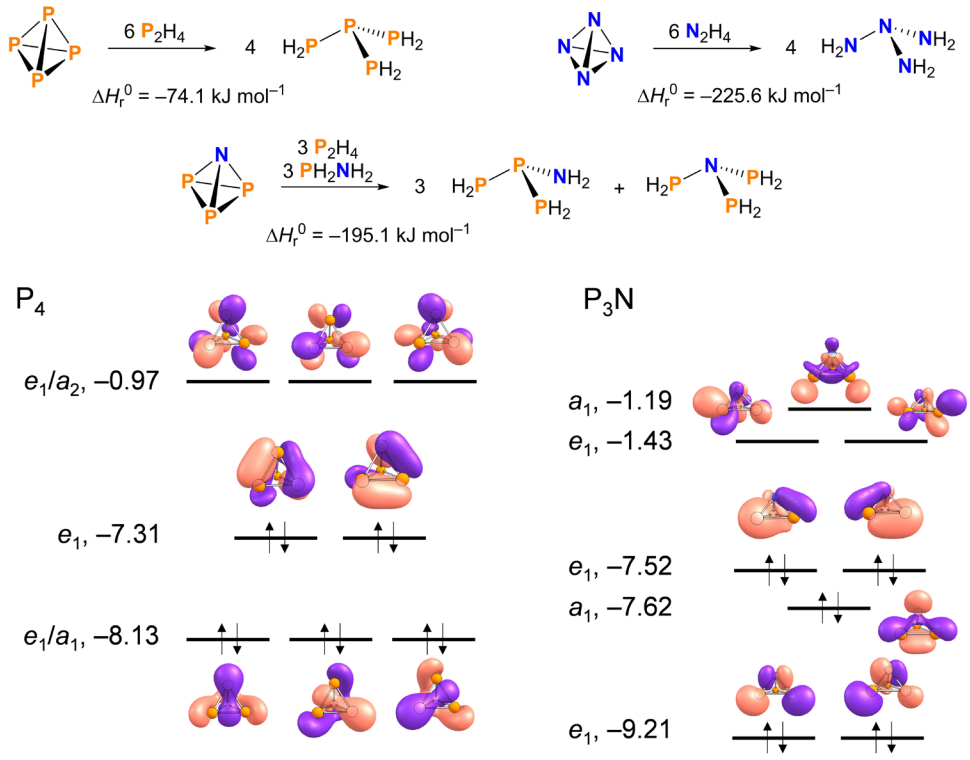

Fig. 4. Calculated strain energies in tetrahedral N_4 (1), P_4 (2), and P_3N (10) and frontier molecular orbitals of P_4 (2) and P_3N (10) using C_{3v} symmetry to allow for direct comparison of the calculated orbitals. The strain energies are calculated via the homodesmotic equations depicted on top at the CBS–QB3//B3LYP/cc–pVTZ and the molecular orbitals at B3LYP/cc–pVTZ level of theory. Orbital energies are given in eV. Atoms are color coded in black (hydrogen), blue (nitrogen), and orange (phosphorus).

molecule is relatively unstrained. At CBS-QB3//B3LYP/cc–pVTZ level of theory, a ring strain energy of 74.1 kJ mol^{-1} is obtained. This is lower than the calculated strain energy in N_4 (**1**) (225.6 kJ mol^{-1}). Note that the frontier orbitals in phosphorus as a heavier *p*-block element are more diffuse and the propensity for lone pairs to accumulate *s* orbital character (*33*). The incorporation of only one nitrogen atom into the P_4 (**2**) tetrahedron increases the strain energy in P_3N (**10**) to 195.1 kJ mol^{-1}. This is in a same region as the previously reported strain energy in P_3CH (**9**) (156.2 kJ mol^{-1}) (*26*), which is higher than that of cyclopropane (119.6 kJ mol^{-1}) (*34*). These results are in agreement with our calculated dissociation reaction enthalpies for various P/N tetrahedrons (table S9). Thermally, white phosphorus (P_4) only dissociates above 1100 K into two molecules of P_2 (*35*), which is reflected in a calculated highly endothermic reaction enthalpy of 236.0 kJ mol^{-1} at the CBS–QB3//B3LYP/cc–pVTZ level of theory. The reaction for the dissociation of P_3N into PN and P_2 is also endothermic (122.1 kJ mol^{-1}), thus underlining the stability of the P_3N tetrahedron. By incorporating more nitrogen atoms in the tetrahedron scaffold, the dissociation reactions of P_2N_2, PN_3, and N_4 become highly exothermic and energetically favored (table S9).

Last, we are proposing potential formation routes to P_3N (**10**). Electronic structure calculations revealed that three H_2NP_3 isomers (Fig. 5 and fig. S3) might act as reactive intermediates. Among four H_2NP_3 isomers **13** to **16**, **13** to **15** could undergo unimolecular decomposition via molecular hydrogen loss and simultaneous ring closure to P_3N (**10**). These pathways involve transition states located 345.3 kJ mol^{-1} (3.58 eV) to 391.7 kJ mol^{-1} (4.06 eV) above the energy of the reactant, which could be overcome through kinetic energy transfer from the impinging electrons to isomers **13** to **15** (*36*). Note that no one-step decomposition-isomerization mechanism was located for the acyclic isomer **16**, suggesting that a cyclic, pnictide-based triatomic moiety represents a requirement to form P_3N (**10**). Ion counts for H_2NP_3 and $H_2{}^{15}NP_3$ (fig. S4) were identified in the sublimation phase of the exposed PH_3-N_2 ices at a PE = 10.49 eV. However, the intensity of the ion counts even at 10.49 eV is too low to determine the nature of their structural isomers through the reduction of the PE. Nevertheless, the computed pathways suggest plausible routes, involving precursor molecules carrying a cyclic P_3 moiety (**13** and **16**) to form P_3N (**10**) via nonequilibrium chemistry triggered by electron exposure of PH_3-N_2 ices.

DISCUSSION

To sum up, the identification of the tetrahedral molecule 1,2,3-triphospha-4-azatricyclo [1.1.0.$0^{2,4}$] butane (P_3N, **10**) progresses our fundamental understanding of the chemical bonding of highly strained binary pnictogen molecules carrying nitrogen and phosphorus and affords a formidable strategy to prepare traditionally "nonexisting" interpnictides such as PN_3 and P_2N_2 via nonequilibrium chemistry, which have escaped any preparation and spectroscopic detection thus far. A "radical" approach to a "P_3 transfer chemistry" (*26*) or the controlled combination of diphosphorus (P_2) (*37*, *38*), diphosphatriazolate anion ($P_2N_3^-$) (*39*, *40*), and phosphorus mononitride (PN) (*41*, *42*) in solution might enable a preparative synthesis and isolation of molecular P_3N (**10**) in the future.

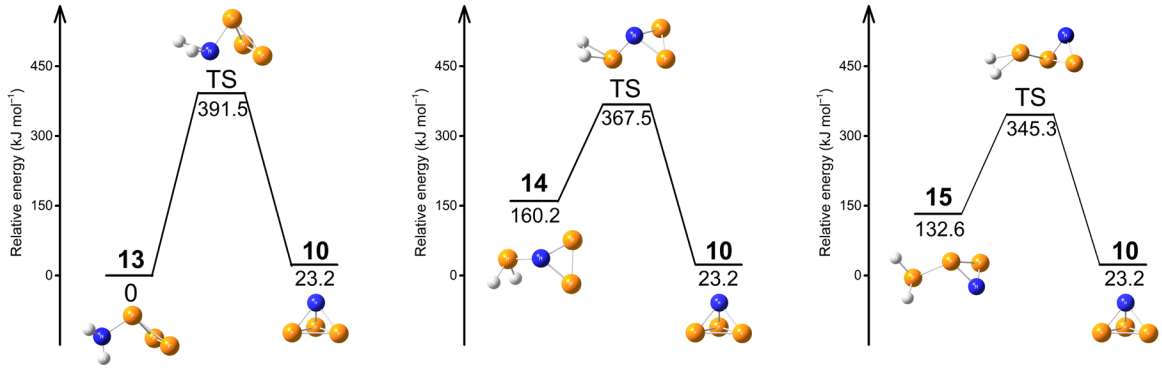

Fig. 5. Potential energy surfaces of distinct H_2P_3N reaction intermediates (13 to 15) undergoing molecular hydrogen loss to 1,2,3-triphospha-4-azatricyclo [1.1.0.0^{2,4}] butane (P_3N, 10). The energies are computed at the CCSD(T)/CBS//B3LYP/cc–pVTZ + ZPVE level of theory. Atoms are color coded in white (hydrogen), blue (nitrogen), and orange (phosphorus). TS indicates the transition state.

MATERIALS AND METHODS

Experimental methods

The experiments were carried out in an ultrahigh vacuum chamber pumped to a base pressure of 7×10^{-11} torr using turbomolecular pumps (Osaka, TG1300MUCWB and TG420MCAB) backed with oil-free scroll pumps (Edwards, GVSP30). Within the chamber, a fine-polished silver wafer is mounted to a copper cold head cooled by a closed-cycle helium refrigerator (Sumitomo Heavy Industries, RDK-415E) capable of achieving temperatures to 5.0 ± 0.1 K. The wafer can be translated vertically and rotated in the horizontal plane with a linear translator (McAllister, BLT106) and rotational feedthrough (Thermionics Vacuum Products, RNN-600/FA/MCO), respectively. During the experiment, phosphine (PH_3, Sigma-Aldrich; 99.9995%) and nitrogen (N_2, Matheson; 99.9992%) [or 15-nitrogen ($^{15}N_2$, Sigma-Aldrich; 98% ^{15}N)] gases were co-deposited onto the silver wafer via two separate glass capillary arrays to produce ice mixtures of PH_3 and N_2 with a composition ratio of (1.2 ± 0.2):1. The ice thickness was determined via exploiting laser interferometry (*43*) by monitoring the interference fringes of a 632.8-nm helium-neon laser (CVI Melles Griot, 25-LHP-230) that is reflected from the silver wafer (2° relative to the ice surface normal). With the refractive indexes of pure PH_3 and N_2 ices (n_{PH_3} = 1.51 ± 0.04, n_{N_2} = 1.21 ± 0.01) (*43*, *44*) and their composition ratio [PH_3 and N_2 = (1.2 ± 0.2):1], the thickness of the ice mixture was estimated to be 1000 ± 50 nm.

After the deposition, the ices were examined using a Fourier transform infrared (FTIR) spectrometer (Nicolet 6700; 6000 to 400 cm^{-1}, 4 cm^{-1} spectral resolution). The ice composition was calculated using a modified Beer-Lambert law. For PH_3, on the basis of the absorption coefficients for the 2319 cm^{-1} (ν_1/ν_1; 4.7×10^{-18} cm molecule^{-1}) and 983 cm^{-1} (ν_2; 5.1×10^{-19} cm molecule^{-1}) bands along with corresponding integrated areas, its average column density was determined to be $(1.5 \pm 0.3) \times 10^{18}$ molecules cm^{-2}, which can be converted to 550 ± 60 nm thick ice with the density of PH_3 ice (0.9 g cm^{-3}). Considering the thickness of the total ice (1000 ± 50 nm) and PH_3 ice (550 ± 60 nm), the thickness of N_2 was estimated to be 450 ± 50 nm, which corresponds to a column density of $(1.2 \pm 0.3) \times 10^{18}$ molecules cm^{-2}, taking into account the densities of N_2 ice (0.94 ± 0.02 g cm^{-3}). Therefore, the ratio of PH_3 and N_2 was found to be (1.2 ± 0.2):1.

The ices were then isothermally processed by 5 keV electrons (Specs EQ 22-35 electron source) at 5.0 ± 0.1 K for 2 hours at currents of 0 nA (blank) and 100 nA. The electron incidence angle is 70° to the ice surface normal. Using Monte Carlo simulations (CASINO 2.42) (*45*), the maximum and average depths of the electrons were estimated to be 880 ± 90 nm and 490 ± 50 nm, respectively, which are less than the ice thickness (1000 ± 50 nm), avoiding interaction between the electrons and the silver wafer (table S3). The irradiation doses were determined to be 26 ± 4 eV per PH_3 molecule and 21 ± 3 eV per N_2 molecule. To monitor the evolution of the ices during the electron irradiation, in situ FTIR spectra were recorded at intervals of 2 min.

After the irradiation, the ices were annealed to 300 K at 1 K min^{-1} (TPD), exploiting a programmable temperature controller (Lakeshore 336). During the TPD phase, the subliming molecules from the ices were examined using a ReTOF mass spectrometer (Jordon TOF Products Inc.) coupled with tunable VUV photon ionization (table S4). Two PEs of 10.49 and 8.53 eV were selected to distinguish the P_3N distinct isomers. The 10.49 eV (118.222 nm) laser was generated via frequency tripling ($\omega_{vuv} = 3\omega_1$) of the third harmonic (355 nm) of the fundamental (1064 nm) of a neodymium-doped yttrium aluminum garnet (Nd:YAG) laser using xenon (Xe) as a nonlinear medium. To produce 8.53 eV (145.351 nm) light, the second harmonic (532 nm) of an Nd:YAG laser was used to pump a Rhodamine 610/640 dye mixture [ethanol (0.17/0.04 g liter^{-1})] to obtain 606.948 nm (2.04 eV) (Sirah, Cobra-Stretch), which underwent a frequency tripling process to achieve ω_1 = 202.316 nm (6.13 eV) [β-BaB_2O_4 (BBO) crystals, 44° and 77°]. A second Nd:YAG laser (second harmonic at 532 nm) pumped the dichloromethane dye [dimethyl sulfoxide (0.30 g liter^{-1})] to obtain ω_2 = 665 nm (1.86 eV), which underwent a frequency doubling process to achieve ω_2 = 332.5 nm (3.73 eV) [β-BaB_2O_4 (BBO) crystals, 44°] and then combined with $2\omega_1$, generating ω_{vuv} = 8.53 eV (145.351 nm) at 1012 photons per pulse via difference four-wave mixing ($\omega_{vuv} = 2\omega_1 - \omega_2$) in pulsed gas jets of krypton (Kr) (table S4). The VUV photons were spatially separated from the incident lasers ($2\omega_1$ and ω_2) and other wavelengths generated via multiple resonant and nonresonant processes ($2\omega_1 + \omega_2$; $3\omega_1$; $3\omega_2$) using a biconvex lens made with lithium fluoride (LiF) (ISP Optics) and directed 2 mm above the ice surface for ionizing the sublimed species. The ionized molecules were examined with the ReTOF mass spectrometer based on their arrival time to an MCP, which is correlated with *m*/*z*. The MCP signal was first amplified by a fast preamplifier (ORTEC 9305) and then recorded using a multichannel scalar (MCS) (FAST ComTec, P7888-1 E).

The MCS is triggered with a pulse generator (Quantum Composers 9518) at 30 Hz. Each final mass spectrum is the average of 3600 sweeps of the flight time in 4 ns bin width and correlates to a 2 K increase of the sample temperature.

Computational methods

All computations were carried out with Gaussian 16, Revision C.01 (table S5 and S6) (*46*). For geometry optimizations and frequency computations, the density functional theory B3LYP functional (*47*–*49*) was used, using the Dunning correlation-consistent split valence basis set cc–pVTZ (*50*). On the basis of these geometries, the corresponding frozen-core coupled clusters (*51*–*54*) CCSD(T)/cc–pVDZ, CCSD(T)/cc–pVTZ, and CCSD(T)/cc–pVQZ single-point energies were computed and extrapolated to complete the basis set limit (*55*) CCSD(T)/CBS with B3LYP/cc–pVTZ ZPVE corrections. The adiabatic IEs were computed by taking the ZPVE-corrected energy difference between the neutral and ionic species that correspond to similar conformations. As in general, the difference of ^{14}N and ^{15}N isotopologues in the ZPVE is marginal. We used the ZPVEs of ^{14}N isotopologues for IEs calculation and assume them as the same for our experiments with heavier isotopologues. The electric field of the extractor plate of our experimental setup lowers the IE by up to 0.03 eV. For the calculation of the strain energies depicted in Fig. 4, all geometries were optimized at B3LYP/cc-pVTZ level of theory and augmented CBS-QB3 (*56*) energies.

SUPPLEMENTARY MATERIALS

Supplementary material for this article is available at https://science.org/doi/10.1126/sciadv.abo5792

REFERENCES AND NOTES

1. F. Krafft, Phosphorus. From elemental light to chemical element. *Angew. Chem. Int. Ed.* **8**, 660–671 (1969).
2. L. R. Maxwell, S. B. Hendricks, V. M. Mosley, Electron diffraction by gases. *J. Chem. Phys.* **3**, 699–709 (1935).
3. M. T. Nguyen, T. L. Nguyen, A. M. Mebel, R. Flammang, Azido-nitrene is probably the N_4 molecule observed in mass spectrometric experiments. *J. Phys. Chem. A* **107**, 5452–5460 (2003).
4. A. Bettendorff, Allotropische zustände des arsens. *Justus Liebigs Ann. Chem.* **144**, 110–114 (1867).
5. Y. Morino, T. Ukaji, T. Ito, Molecular structure determination by gas electron diffraction at high temperatures. I. Arsenic. *Bull. Chem. Soc. Jpn.* **39**, 64–71 (1966).
6. G. M. Rosenblatt, The composition of antimony vapor. *J. Phys. Chem.* **66**, 2259–2260 (1962).
7. T. A. Engesser, W. J. Transue, P. Weis, C. C. Cummins, I. Krossing, As–P vs. P–P insertion in AsP_3: Kinetic control of the formation of $[AsP_3NO]^+$. *Eur. J. Inorg. Chem.* **2019**, 2607–2612 (2019).
8. P. Weis, D. C. Rohner, R. Prediger, B. Butschke, H. Scherer, S. Weber, I. Krossing, First experimental evidence for the elusive tetrahedral cations $[EP_3]^+$ (E = S, Se, Te) in the condensed phase. *Chem. Sci.* **10**, 10779–10788 (2019).
9. D. Opalka, L. V. Poluyanov, W. Domcke, Relativistic Jahn-Teller effects in the photoelectron spectra of tetrahedral P_4, As_4, Sb_4, and Bi_4. *J. Chem. Phys.* **135**, 104108 (2011).
10. P. Jerabek, G. Frenking, Comparative bonding analysis of N_2 and P_2 versus tetrahedral N_4 and P_4. *Theor. Chem. Acc.* **133**, 1447 (2014).
11. S. Urpelainen, J. Niskanen, J. A. Kettunen, M. Huttula, H. Aksela, Valence photoionization and resonant Auger decay of Sb_4 clusters at resonances below the *4d* ionization threshold. *Phys. Rev. A* **83**, 015201 (2011).
12. J. A. Kettunen, S. Urpelainen, S. Heinäsmäki, M. Huttula, Dissociation of As_4 clusters following valence photoionization and *3d* core excitation. *Phys. Rev. A* **86**, 023201 (2012).
13. S. Rayne, K. Forest, Binary mixed carbon, silicon, nitrogen, and phosphorus cubane derivatives as potential high energy materials. *Comput. Theor. Chem.* **1080**, 10–15 (2016).
14. A. Hirsch, Z. Chen, H. Jiao, Spherical aromaticity of inorganic cage molecules. *Angew. Chem. Int. Ed.* **40**, 2834–2838 (2001).
15. P. V. R. Schleyer, C. Maerker, A. Dransfeld, H. Jiao, N. J. R. van Eikema Hommes, Nucleus-independent chemical shifts: A simple and efficient aromaticity probe. *J. Am. Chem. Soc.* **118**, 6317–6318 (1996).
16. F. Cacace, G. de Petris, A. Troiani, Experimental detection of tetranitrogen. *Science* **295**, 480–481 (2002).
17. O. Kwon, P. M. Almond, M. L. McKee, Structures and reactions of P_2N_2: A hybrid of elemental N_2 and P_4? *J. Phys. Chem. A* **106**, 6864–6870 (2002).
18. L. Wang, P. L. Warburton, P. G. Mezey, A theoretical study of nitrogen-rich phosphorus nitrides $P(N_n)_m$. *J. Phys. Chem. A* **109**, 1125–1130 (2005).
19. G. A. Ozin, High-temperature gas-phase laser Raman spectroscopy: Evidence for the existence and molecular structure of the interpnictides As_3P, As_2P_2, and AsP_3 in mixtures of phosphorus and arsenic vapours and SbP_3 in mixtures of phosphorus and antimony vapours. *J. Chem. Soc. A* , 2307–2310 (1970).
20. N. A. Piro, C. C. Cummins, P_2 addition to terminal phosphide M≡P triple bonds: A rational synthesis of *cyclo*-P_3 complexes. *J. Am. Chem. Soc.* **130**, 9524–9535 (2008).
21. B. M. Cossairt, M.-C. Diawara, C. C. Cummins, Facile synthesis of AsP_3. *Science* **323**, 602–602 (2009).
22. N. A. Piro, C. C. Cummins, Tetraphosphabenzenes obtained via a triphosphacyclobutadiene intermediate. *Angew. Chem. Int. Ed.* **48**, 934–938 (2009).
23. N. A. Piro, thesis, Massachusetts Institute of Technology, Cambridge, MA (2009).
24. B. M. Cossairt, C. C. Cummins, Properties and reactivity patterns of AsP_3: An experimental and computational study of group 15 elemental molecules. *J. Am. Chem. Soc.* **131**, 15501–15511 (2009).
25. B. M. Cossairt, C. C. Cummins, A. R. Head, D. L. Lichtenberger, R. J. F. Berger, S. A. Hayes, N. W. Mitzel, G. Wu, On the molecular and electronic structures of AsP_3 and P_4. *J. Am. Chem. Soc.* **132**, 8459–8465 (2010).
26. M. Y. Riu, M. Ye, C. C. Cummins, Alleviating strain in organic molecules by incorporation of phosphorus: Synthesis of triphosphatetrahedrane. *J. Am. Chem. Soc.* **143**, 16354–16357 (2021).
27. Y. Valadbeigi, Phosphorus-doped nitrogen clusters (N_nP_m): Stable high energy density materials. *Chem. Phys. Lett.* **645**, 195–199 (2016).
28. A. M. Turner, R. I. Kaiser, Exploiting photoionization reflectron time-of-flight mass spectrometry to explore molecular mass growth processes to complex organic molecules in interstellar and solar system ice analogs. *Acc. Chem. Res.* **53**, 2791–2805 (2020).
29. C. Zhu, A. K. Eckhardt, S. Chandra, A. M. Turner, P. R. Schreiner, R. I. Kaiser, Identification of a prismatic P_3N_3 molecule formed from electron irradiated phosphine-nitrogen ices. *Nat. Commun.* **12**, 5467 (2021).
30. G. Socrates, *Infrared and Raman Characteristic Group Frequencies: Tables and Charts* (Wiley, 2004).
31. K. K. Irikura, R. D. Johnson, R. N. Kacker, R. Kessel, Uncertainties in scaling factors for ab initio vibrational zero-point energies. *J. Chem. Phys.* **130**, 114102 (2009).
32. P. Pyykkö, Additive covalent radii for single-, double-, and triple-bonded molecules and tetrahedrally bonded crystals: A summary. *J. Phys. Chem. A* **119**, 2326–2337 (2015).
33. Y. Naruse, S. Inagaki, in *Orbitals in Chemistry*, S. Inagaki, Ed. (Springer Berlin Heidelberg, 2010), pp. 265–291.
34. R. D. Bach, O. Dmitrenko, The effect of carbonyl substitution on the strain energy of small ring compounds and their six-member ring reference compounds. *J. Am. Chem. Soc.* **128**, 4598–4611 (2006).
35. H. Bock, H. Mueller, Gas-phase reactions. 44. The phosphorus $P_4 \leftrightarrow 2P_2$ equilibrium visualized. *Inorg. Chem.* **23**, 4365–4368 (1984).
36. B. M. Jones, R. I. Kaiser, Application of reflectron time-of-flight mass spectroscopy in the analysis of astrophysically relevant ices exposed to ionization radiation: Methane (CH_4) and D_4-methane (CD_4) as a case study. *J. Phys. Chem. Lett.* **4**, 1965–1971 (2013).
37. N. A. Piro, J. S. Figueroa, J. T. McKellar, C. C. Cummins, Triple-bond reactivity of diphosphorus molecules. *Science* **313**, 1276–1279 (2006).
38. A. Velian, M. Nava, M. Temprado, Y. Zhou, R. W. Field, C. C. Cummins, A retro Diels–Alder route to diphosphorus chemistry: Molecular precursor synthesis, kinetics of P_2 transfer to 1,3-dienes, and detection of P_2 by molecular beam mass spectrometry. *J. Am. Chem. Soc.* **136**, 13586–13589 (2014).
39. A. Velian, C. Cummins Christopher, Synthesis and characterization of $P_2N_3^-$: An aromatic ion composed of phosphorus and nitrogen. *Science* **348**, 1001–1004 (2015).
40. G. L. Hou, B. Chen, W. J. Transue, D. A. Hrovat, C. C. Cummins, W. T. Borden, X. B. Wang, Negative ion photoelectron spectroscopy of $P_2N_3^-$: Electron affinity and electronic structures of $P_2N_3^{\cdot}$. *Chem. Sci.* **7**, 4667–4675 (2016).
41. A. Eckhardt, M.-L. Riu, M. Ye, P. Mueller, G. Bistoni, C. Cummins, Taming phosphorus mononitride (PN) (ChemRxiv, 2021); https://doi.org/10.33774/chemrxiv-2021-zxtmf.
42. J. L. Martinez, S. A. Lutz, D. M. Beagan, X. Gao, M. Pink, C. H. Chen, V. Carta, P. Moenne-Loccoz, J. M. Smith, Stabilization of the dinitrogen analogue, phosphorus nitride. *ACS Cent. Sci.* **6**, 1572–1577 (2020).
43. A. M. Turner, M. J. Abplanalp, S. Y. Chen, Y. T. Chen, A. H. Chang, R. I. Kaiser, A photoionization mass spectroscopic study on the formation of phosphanes in low temperature phosphine ices. *Phys. Chem. Chem. Phys.* **17**, 27281–27291 (2015).

44. R. Luna, M. Á. Satorre, M. Domingo, C. Millán, C. Santonja, Density and refractive index of binary CH_4, N_2 and CO_2 ice mixtures. *Icarus* **221**, 186–191 (2012).
45. D. Drouin, A. R. Couture, D. Joly, X. Tastet, V. Aimez, R. Gauvin, CASINO V2.42—A fast and easy-to-use modeling tool for scanning electron microscopy and microanalysis users. *Scanning* **29**, 92–101 (2007).
46. M. J. Frisch, G. W. Trucks, H. B. Schlegel, G. E. Scuseria, M. A. Robb, J. R. Cheeseman, G. Scalmani, V. Barone, G. A. Petersson, H. Nakatsuji, X. Li, M. Caricato, A. V. Marenich, J. Bloino, B. G. Janesko, R. Gomperts, B. Mennucci, H. P. Hratchian, J. V. Ortiz, A. F. Izmaylov, J. L. Sonnenberg, Williams, F. Ding, F. Lipparini, F. Egidi, J. Goings, B. Peng, A. Petrone, T. Henderson, D. Ranasinghe, V. G. Zakrzewski, J. Gao, N. Rega, G. Zheng, W. Liang, M. Hada, M. Ehara, K. Toyota, R. Fukuda, J. Hasegawa, M. Ishida, T. Nakajima, Y. Honda, O. Kitao, H. Nakai, T. Vreven, K. Throssell, J. A. Montgomery Jr., J. E. Peralta, F. Ogliaro, M. J. Bearpark, J. J. Heyd, E. N. Brothers, K. N. Kudin, V. N. Staroverov, T. A. Keith, R. Kobayashi, J. Normand, K. Raghavachari, A. P. Rendell, J. C. Burant, S. S. Iyengar, J. Tomasi, M. Cossi, J. M. Millam, M. Klene, C. Adamo, R. Cammi, J. W. Ochterski, R. L. Martin, K. Morokuma, O. Farkas, J. B. Foresman, D. J. Fox, *Gaussian 16 Rev. C.01* (2016).
47. A. D. Becke, Density-functional exchange-energy approximation with correct asymptotic behavior. *Phys. Rev. A* **38**, 3098–3100 (1988).
48. C. Lee, W. Yang, R. G. Parr, Development of the colle-salvetti correlation-energy formula into a functional of the electron density. *Phys. Rev. B* **37**, 785–789 (1988).
49. A. D. Becke, Density-functional thermochemistry. III. The role of exact exchange. *J. Chem. Phys.* **98**, 5648–5652 (1993).
50. T. H. Dunning, Gaussian basis sets for use in correlated molecular calculations. I. The atoms boron through neon and hydrogen. *J. Chem. Phys.* **90**, 1007–1023 (1989).
51. R. J. Bartlett, J. D. Watts, S. A. Kucharski, J. Noga, Non-iterative fifth-order triple and quadruple excitation energy corrections in correlated methods. *Chem. Phys. Lett.* **165**, 513–522 (1990).
52. J. Čížek, On the correlation problem in atomic and molecular systems. Calculation of wavefunction components in ursell-type expansion using quantum-field theoretical methods. *J. Chem. Phys.* **45**, 4256–4266 (1966).
53. K. Raghavachari, Electron correlation techniques in quantum chemistry: Recent advances. *Annu. Rev. Phys. Chem.* **42**, 615–642 (1991).
54. J. F. Stanton, Why CCSD(T) works: A different perspective. *Chem. Phys. Lett.* **281**, 130–134 (1997).
55. K. A. Peterson, D. E. Woon, T. H. Dunning, Benchmark calculations with correlated molecular wave functions. IV. The classical barrier height of the $H+H_2 \rightarrow H_2+H$ reaction. *J. Chem. Phys.* **100**, 7410–7415 (1994).
56. J. A. Montgomery, M. J. Frisch, J. W. Ochterski, G. A. Petersson, A complete basis set model chemistry. VII. Use of the minimum population localization method. *J. Chem. Phys.* **112**, 6532–6542 (2000).
57. S. G. Lias, Ionization energy evaluation, in *NIST Chemistry WebBook* (NIST Standard Reference Database Number 69, 2022); https://doi.org/10.18434/T4D303.
58. D. C. Frost, S. T. Lee, C. A. McDowell, The photoelectron spectrum of HCP and comments on the first photoelectron band of HCN. *Chem. Phys. Lett.* **23**, 472–475 (1973).
59. A. M. Turner, S. Chandra, R. C. Fortenberry, R. I. Kaiser, A photoionization reflectron time-of-flight mass spectrometric study on the detection of ethynamine ($HCCNH_2$) and 2H-azirine (c-H_2 CCHN). *ChemPhysChem* **22**, 985–994 (2021).

Acknowledgments

Funding: This work was supported by the U.S. National Science Foundation (NSF) under grant AST 2103269 to The University of Hawaii (to C.J.Z., C.Z., and R.I.K.). A.K.E. acknowledges the Alexander von Humboldt-Foundation for a Feodor Lynen Return Fellowship. **Author contributions:** R.I.K. designed the experiments. C.Z. and C.J.Z. performed experiments and analyzed the data. A.K.E. carried out the theoretical analysis. C.J.Z., A.K.E., and R.I.K. wrote the manuscript, which was read, revised, and approved by all coauthors. **Competing interests:** The authors declare that they have no competing interests. **Data and materials availability:** All data needed to evaluate the conclusions in the paper are present in the paper and/or the Supplementary Materials.

Submitted 12 February 2022
Accepted 13 April 2022
Published 1 June 2022
10.1126/sciadv.abo5792